2024 IEEE International Conference on Robotics and Automation (ICRA 2024)
May 13-17, 2024. Yokohama, Japan

Low-to-High Resolution Path Planner for Robotic Gas Distribution Mapping

Rohit V. Nanavati[1], Callum Rhodes[2], Matthew J. Coombes[1] and Cunjia Liu[1]

***Abstract*— Robotic gas distribution mapping improves the understanding of a hazardous gas dispersion while putting the human operator out of danger. Generating an accurate gas distribution map quickly is of utmost importance in situations such as gas leaks and industrial incidents, so that the efficient use of resources in response to incidents can be facilitated. In this paper, to incorporate the operational requirement on map granularity, we propose a low-to-high resolution path planner that first guides a single robots to quickly and sparsely sample the region of interest to generate a low resolution gas distribution map, followed by high resolution sampling informed by the low resolution map as a prior. The low resolution prior acts as a coverage survey allowing the algorithm to perform a relatively exploitative search of high concentration regions, resulting in overall shorter mission times. The proposed framework is designed to iteratively identify the next best T locations to sample, which prioritises the potentially high reward locations, while ensuring that the robot can travel to and sample the chosen locations within a user specified map update cycle. We present a simulation study to demonstrate the alternating exploration-exploitation like behaviour along with bench-marking its performance in contrast to the traditional sampling path planners and various reward functions.**

I. Introduction

Information about the distribution of harmful gases in an environment can be critical in determining and executing rescue and maintenance operations from a disaster management perspective. Gas Distribution Mapping (GDM) is a field of research to generate a map of gas concentration in a given operational area primarily to identify high/low concentration regions along with potential sources of gas leakage [1]. Such a map can be generated using various mapping tools from a set of point measurements obtained by a network of strategically placed static sensors or a mobile sensor. The mobile-sensor based scheme allows a set of spatially diverse measurements to be collected in a timely manner even comparing to a relatively high number of static senors.

The GDM literature consist of various data driven methods of generating a distribution map without assumptions about the underlying dispersion models. Data driven mapping solutions [2]–[8] primarily fit and interpolate the sampled data to a densely distributed function. One of the early data-driven mapping solution was proposed in [2], called Kernel DM, which represents the operational area as a grid of cells represented with mean concentration along with the use of Gaussian density functions to weight the effects of measurement samples away from the sampling location. There have been multiple variants of the Kernel DM method in the literature like the Kernel DM+V [3], Kernel DM+V/W [4], and TD Kernel DM+V/W [5]. These variants additionally generate variability maps over the grid and account for wind effects and time decay associated with the quality of measurements. Another data driven method models the gas distribution as a Gaussian process (GP) or a mixture of GPs [6], [7]. A GP based mapping solution assumes a prior map and incorporates sampled data to generate a posterior estimate of the concentration map along with the associated uncertainty. Gaussian Markov random field (GMRF) based mapping algorithms have also been proposed in [8] which can be regarded as numerically approximated GPs over grid points [9]. In addition to the underlying mapping tool, for online robotic GDM tasks, the choice of sampling location is equally as important for improving the efficiency and accuracy of GDP. Therefore, a path planning solution that efficiently covers an operational region and evolves based on the current belief of the gas distribution is desirable.

In the literature, early path planning solutions used for GDM applications are usually non-adaptive in nature, that is, the robot trajectories are predefined. The most commonly used path planning solution is a sweeping motion over the operational area [10]–[12]. There have been few works like [13]–[16] that focus on informative path planning solutions. The path planning algorithm presented in [13] employed a artificial potential field based technique to decide the next sampling location and demonstrated that the informative path planning solution resulted in quicker convergence to a meaningful gas distribution map as compared a predefined sweeping trajectory. Moreover, [16] tested various information path planning reward function using the mean concentration and variance maps generated using the GMRF model. The reward functions were aimed at maximising the information gain while penalising the distance of the potential future sampling location. Another study that analyzed multiple path planning algorithms for 3D GDM was presented in [14]. In [14], the performance of three path planning solutions namely - Levy flight, Entropy strategy, and Kullback-Liebler Divergence Strategy - were analyzed along with a clustering algorithm that divided the operational region in k clusters which are sequentially visited by the robot. It was found that the three path planning solutions were able to generate high quality maps for small areas of the operational region as they do not favour exploratory behaviour, and thus achieving higher map detail over some parts of the map. Furthermore, the informative strategies proposed in [14]–[16] were designed to

[1]Center of Autonomous Systems, Department of Aeronautical and Automotive Engineering, Loughborough University, United Kingdom. {r.nanavati,m.j.coombes,c.liu5}@lboro.ac.uk
[2] Department of Computing, Imperial College London, United Kingdom. c.rhodes@imperial.ac.uk

choose the next sampling location for a single time step into the future. A path planner that balances some exploitative and exploratory properties with a relatively longer planning horizon could be beneficial in resolving the complete map.

Most of the discussed path planning algorithms for robotic GDM aim to produce a complete map at the end of the mission. However, in certain operations, the end-users may want to periodically extract the best available map during the mission to inform their decision-making process, and thus the map in progress should have both reasonable overall coverage and a refined granularity at key areas. In this case, the need to balance exploration and exploitation simultaneously becomes much more critical to effectively cover and investigate the mapping domain, but distributing the mapping tasks over phases may simplify the design problem.

In the light of this discussion, we propose low-to-high resolution (LHR) GDM framework that first performs a sparse sampling survey of the environment to construct a low resolution map estimate as quick as possible, which can serve as a prior to the second phase of high resolution sampling. We use a GMRF based map representation [8] along with an efficient Gaussian belief propagation solver [17] to resolve the map using the collected measurements. The low resolution map effectively sparsely identifies potential high concentration regions, which enables the high resolution sampling phase to perform exploitative dense sampling over the identified focus region. The high resolution mapping aims to update the estimated map within a user specified interval using measurements obtained over a finite horizon. The path planer therefore needs to find a viable path that can maximise the information collected while respecting the time budget, resulting in a faster mapping of high concentration regions. It will be shown that such a design alternates between exploitative dense sampling and spatially diverse sampling to quickly resolve the map. We demonstrate the performance of the LHR-GDM framework using a illustrative simulation study along with a comparison study with baseline algorithms such as sweep based planning and constrained random sampling methods, as well as the performance with different reward functions.

II. Preliminaries and problem formulation

Consider a robotic platform in a closed operating region denoted by $\mathcal{D} \subset \mathbb{R}^2$. The operating region is assumed to be an obstacle free open space. The region $\mathcal{D}$ is discretised into uniform grid cells with a prespecified resolution denoted by d_{res}. Note that d_{res} is the smallest acceptable resolution for the gas distribution map. Let $\mathcal{Q} = \{q_1, q_2, \ldots, q_N\}$ denote a set of random variables to be inferred with q_i corresponding to the concentration at the center of the i^{th} cell in $\mathcal{D}$. Moreover, let a measurement obtained by a robotic platform at the i^{th} cell be denoted as z_i. It is assumed that the robotic platform samples the center of the cell to obtain a gas measurement corresponding to the cell. Furthermore, the overall measurement vector containing all the measurements obtained by the robot since the beginning of the mission be denoted as $\boldsymbol{Z}$. The robotic platform is assumed to travel at a constant speed, V, when travelling from one cell to another. Additionally, the platform needs to stop at each cell for t_{sam} seconds to obtain a time-averaged measurement reading.

A. Gaussian Markov random field

We employ a GMRF based inter-cell structure and Gaussian belief propagation based solver to obtain a gas distribution map $\mathcal{M}$ as in [8], [17], [18]. The GMRF factor graph uses Gaussian factors to capture the dependencies between the random variables $\{q_i\}_{1 \to N}$ and its neighbours, the observation likelihood of the gas concentration measured in the i^{th} cell, and, the link to a default background concentration for unsampled cells. Note that the Gaussian variance of the measurement noise for each observation factor is chosen to be proportional to the magnitude of the concentration reading itself. The goal of inference on a GMRF is to find the optimal state vector $\boldsymbol{q}^\star = [q_1, q_2, \ldots, q_N]$, that maximises the posterior of the joint distribution of $\boldsymbol{q}$ conditioned on all available measurements.

$$\boldsymbol{q}^\star = \arg\max_{\boldsymbol{q}} p(\boldsymbol{q}|\boldsymbol{Z}) \tag{1}$$

Typically, the minimum least squares approach is taken to solve this problem, which yields the estimated optimal state vector. From this optimal estimate, the marginal distributions for each variable $q_i \in \boldsymbol{q}^\star$ can be recovered to give the estimated mean concentration value, as well as the associated uncertainty of this prediction, at all discrete points of the mesh. By choosing a probabilistic gas distribution model, the proposed path planner may take advantage of richer information in the map representation. For the full formulation of the GMRF approach to GDM, please refer to [8]. In our work, the Gaussian belief propagation solver in [17] is adopted as a computationally cheap alternative for large scale maps.

B. Problem formulation

The aim of this paper is to design a path planning algorithm (or framework) that can incorporate operational requirements, and autonomously guides the robotic platform in such a fashion that

- the gas distribution map is updated within a user specified fixed time cycle t_{up},
- potentially high concentration regions based on the $\boldsymbol{Z}$ are favoured over other regions, and
- each cell is visited only once.

The constraint of a fixed update cycle is useful for time sensitive applications (like emergency response to gas leaks) as more information collected by the robot can be incorporated to inform a counter-measure action. Therefore, a favourable path planer needs to design a path such that the travel and sampling times are accounted for while obtaining as much information as possible.

III. Low-to-High resolution path planner

To generate any accurate gas distribution map of the desired area $\mathcal{D}$, the ideal path planning solution would require the robot to visit each cell q_i at least once to obtain

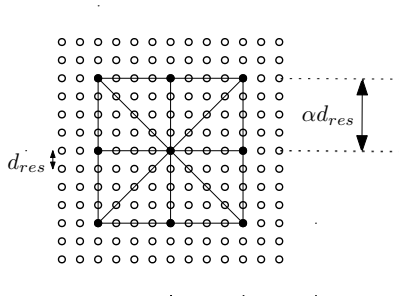

Fig. 1: Structure of the mesh graph $\mathcal{G}_{p,\text{res}}$, where $\circ$ denotes $q_i \in \mathcal{Q}$ and $\bullet$ denotes $q_i \in \mathcal{Q}_s$. Moreover, the edges of $\mathcal{G}_{p,\text{res}}$ are drawn as per (2) for some chosen resolution res.

a measurement sample. However, for a high resolution map of $\mathcal{D}$, the number of locations to visit can be very high and consequently obtaining a path planning solution with a large number of possible locations can be computationally expensive. Furthermore, performing dense sampling operations in potentially low concentration regions would not be as beneficial as dense sampling in high concentration regions. The planner should therefore give more preference to estimated high concentration regions, as compared to low concentration regions.

In this section, we discuss the proposed low-to-high resolution path planner for gas distribution mapping (LHR-GDM) that can incorporate the operational requirement of periodically updated maps, whilst guiding a robotic platform with the objective of autonomously mapping the region of interest $\mathcal{D}$. The LHR-GDM framework can be divided in two phases, namely the low resolution survey (LRS) and high resolution sampling (HRS) phase. The path planning solution for each phase are discussed now.

A. Low resolution survey

The low resolution survey is conducted to generate a prior for the gas distribution by sparsely but diversely sampling the region of interest $\mathcal{D}$. The sampling locations can be determined by the operators based on their domain knowledge. For simplicity, we restrict the choice of these sparse sampling cells to a grid-like structure with the grid unit length chosen to be $\alpha d_{res} > d_{res}$ for some $\alpha \in \mathbb{N} > 1$ as shown in Fig. 1 and the set of these grid points be denoted by $\mathcal{Q}_s$. The path planning solution for the LRS will be carried out by employing the structure of the single travelling salesman problem (TSP) and solved using mixed-integer linear programming framework (MILP) to find the shortest path. Note that a TSP based solution presents a generic path planning solution to sample arbitrary prior sampling locations.

Before defining the MILP problem statement, let an undirected mesh graph denoted by $\mathcal{G}_{LRS} = (\mathcal{Q}_s, \mathcal{E}_l)$ where $\mathcal{Q}_s \subseteq \mathcal{Q}$ are its vertices and its edges given by the set $\mathcal{E}_l = \{q_{ij}\}$. The element q_{ij} is the graph edge defined between the q_i and q_j cell as

$$q_{ij} = \{(q_i, q_j) \in \mathcal{Q}_s \;\mid\; q_i - q_j \in \mathcal{U}\}, \tag{2}$$

where

$$\mathcal{U} = \alpha d_{res} \times \{(\pm 1, 0), (0, \pm 1), (\pm 1, 1), (\pm 1, -1)\}.$$

An example of such a graph structure is shown in Fig. 1. Note that as the graph edges q_{ij} are undirected, q_{ij} and q_{ji} denote the same edge and $\mathcal{E}_l$ contains only one of the above.

Let us denote the distance cost c_{ij} and a binary variable $x_{ij} \in \{0, 1\}$ associated with the edge $q_{ij} \in \mathcal{E}_l$ such that c_{ij} is defined as the Euclidean distance between cell i and j in the 2-D space $\mathcal{D}$. The binary variable $x_{ij} = 0$ denotes that the robot does not travel from cell i to cell j, whereas $x_{ij} = 1$ implies that the edge q_{ij} is traversed by the robot in the optimal solution. Therefore, we can now pose the following linear integer programming problem as described in [19]:

$$\begin{aligned}
&\min \sum_{q_{ij} \in \mathcal{E}_l} c_{ij} x_{ij} \\
&\text{s.t.} \\
&(a) \sum_{q_{ir} \in \mathcal{E}_l} x_{ir} + \sum_{q_{rj} \in \mathcal{E}_l} x_{rj} = 2 \quad \forall \;\; r = 1, 2, 3, \ldots, |\mathcal{Q}_s| \\
&(b) \sum_{i,j \in S} x_{ij} \leq |S| - 1 \quad (3 \leq |S| \leq |\mathcal{Q}_s| - 2,\; S \subset \mathcal{Q}_s)
\end{aligned} \tag{P1}$$

The constraint P1(a) ensures that each cell in $\mathcal{Q}_s$ is visited only once. Moreover, constraint P1(b) ensures that there are no subtours in the optimal solution. The robotic platform can sample all $q_i \in \mathcal{Q}_s$ as per the sequence obtained from the optimal solution of (P1) to construct a low resolution gas distribution map of the environment, denoted by $\mathcal{M}^{\star}_{LRS}$.

B. High resolution sampling

In this subsection, we describe the path planning algorithm for generating a high resolution gas distribution map. As the design constraints require the map to be updated within t_{up} seconds, we design an algorithm to choose a sequence of next sampling cells to maximise the relevant information about the gas distribution in $\mathcal{D}$.

Let $\boldsymbol{p}_o$ denote the robot position and r_i denote the reward assigned to the i^{th} cell at the beginning each map update cycle. The reward r_i can be modelled as a function of the predicted gas concentration and/or associated uncertainty of the i^{th} cell based on $\mathcal{M}^{\star}_{t_{up}}$ obtained from the GMRF based mapping solution discussed in section II-A. At the beginning of the high resolution sampling, it follows that $\mathcal{M}^{\star}_{t_{up}} = \mathcal{M}^{\star}_{LRS}$. Furthermore, the rewards $\{r_i\}_{i \in \mathcal{Q}_u}$ can be sorted in a decreasing order and such a sequence be denoted by $R = \text{SORTED}(\{r_i\}_{i \in \mathcal{Q}_u})$, where $\mathcal{Q}_u = \mathcal{Q} \setminus \mathcal{Q}_s$ refers to set of unsampled cells. The objective here is to find a fixed finite set of sampling locations that maximises the achieved reward while satisfying the time constraints of the map update cycle. To this end, we consider the first M cells of the sorted reward sequence R and construct a set of lists $\Omega = \{T_k\}$ where T_k is a combinatorial list of T cells chosen from first M cells of $\mathcal{Q}_u$. Therefore, one can notice that the set Ω exhaustively contains $\binom{M}{T}$ elements. We can now define the following optimisation problem to

choose the optimal combination of cells to sample within the desired time constraints

$$T_k^\star = \max_{T_k \in \Omega} \sum_{h \in T_k} r_h \quad \text{s.t.} \quad \frac{H(T_k)}{V} \leq t_{up} - T t_{sam}\,, \tag{P2}$$

where $H(T_k)$ refers to the shortest path length that passes through each cell in T_k starting from $\boldsymbol{p}_o$ and ending on the farthest node in T_k from $\boldsymbol{p}_o$, denoted by $\boldsymbol{p}_T$. Consider a completely connected undirected graph $\mathcal{G}_h = \{[\boldsymbol{p}_o, T_k], \mathcal{E}_h\}$ with binary variables $y_{ij} \in \{0,1\}$ associated with $q_{ij} \in \mathcal{E}_h$. Let the robot starting position be indexed as 1 and the cell $\boldsymbol{p}_T$ be denoted by index $T+1$. Therefore, mathematically, one can compute $H(T_k)$ by solving the following modified TSP problem:

$$\begin{aligned} H(T_k) &= \min \sum_{q_{ij} \in \mathcal{E}_h} c_{ij} y_{ij} \\ &\text{s.t.} \\ &(a) \sum_{q_{ir} \in \mathcal{E}_h} y_{ir} + \sum_{q_{rj} \in \mathcal{E}_l} y_{rj} = 2 \quad \forall \quad r = 2, 3, \ldots, T \\ &(b) \sum_{i,j \in S} y_{ij} \leq |S| - 1 \quad (3 \leq |S| \leq T-1) \\ &(c) \sum_{q_{1j} \in \mathcal{E}_h} y_{1j} = 1 \\ &(d) \sum_{q_{j,T+1} \in \mathcal{E}_h} y_{j,T+1} = 1 \end{aligned} \tag{3}$$

The constraints 3(c) and 3(d) ensure that cell $\boldsymbol{p}_o$ and $\boldsymbol{p}_T$ have only one edge in the graph. The rest of the constraints are similar to (P1). Once the optimal T cells are sampled, the set $\mathcal{Q}_s$ is updated to contain all the sampled locations. The proposed framework is summarised in Alg. 1.

Algorithm 1: LHR-GDM Path Planner

Input: $\mathcal{D}$, $\mathcal{G}_{LRS}$, M, T, t_{up}, V

Output: Final gas distribution map

```
Solve Problem (P1) for LRS robot trajectory
Sample Q_s, update Z, Q_u and generate M*_LRS
while Q_u ≠ ∅ do
    Compute R and generate Ω
    Solve (3) for H(T_k) ∀ T_k ∈ Ω
    Solve (P2)
    Sample q_h ∀ h ∈ T*_k, update Z, Q_u and
      Generate M*_{t_up}
end
Final map = M*_{t_up}
```

Remark 1. The first M cells of R are chosen to prioritise the sampling of unsampled cells that are likely to be high reward region as per the gas distribution map or belief. The parameter $T \leq M$ is reasonably chosen based on the onboard computational capabilities as $\binom{M}{T}$ combinations that need to be evaluated for solving the optimisation problem P2. Moreover, the user specified update cycle time needs to satisfy the inequality given by $Tt_{sam} + Td_{res}/V \leq t_{up}$. The aforementioned inequality ensures that the robot can successfully travel to and sample T closest cells to it, where Td_{res} is the shortest distance travelled to visit T cells. Furthermore, a choice of t_{up} satisfying the above inequality will dictate the spatial diversity of cells the robotic platform can sample. A t_{up} closer to the lower bound may result in an empty feasible set that can optimise (P2). Therefore, the authors suggest t_{up} be chosen as Tt_{sam} plus twice the biggest side length of the search region for best results.

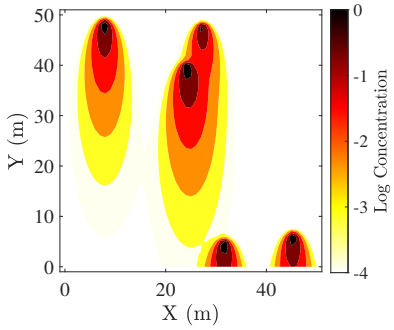

Fig. 2: Ground truth gas distribution in $\mathcal{D}$ with 5 sources.

Remark 2. The MILP problems (P1) and (3) are solved using *the straight algorithm* as explained in [19]. The problem is first solved without the subtour elimination constraints, followed by addition of the necessary violated inequality constraints for any subtours. Such an implementation results in a lower dimensional integer linear programming problem and consequently improves the speed of convergence.

The performance of the algorithm also depends on the choice of the reward function $\{r_i\}_{i \in \mathcal{Q}_u}$, which will be discussed in the next section.

IV. Simulation Study

In this section, the performance of the proposed algorithm in mapping a $50m \times 50m$ region is evaluated using a simulation study. Five sources with different release rates are considered in the operational environment. For generating the ground truth, a Gaussian plume model is used for each release source considering a wind of 3 m/s along the negative Y axis, diffusivity coefficient of 1 m^2/s, and an average particle lifetime of 8s. The randomly source locations and release rate of the sources are tabulated in Table. I.

TABLE I: Source locations and release rates

#Source	Location $\{x_s, y_s\}(m)$	Release rate (g/s)
1	{45.28,6.35}	12.07
2	{31.61,4.87}	12.56
3	{27.34,47.87}	9.39
4	{7.88,48.52}	12.82
5	{24.26,40.0}	12.78

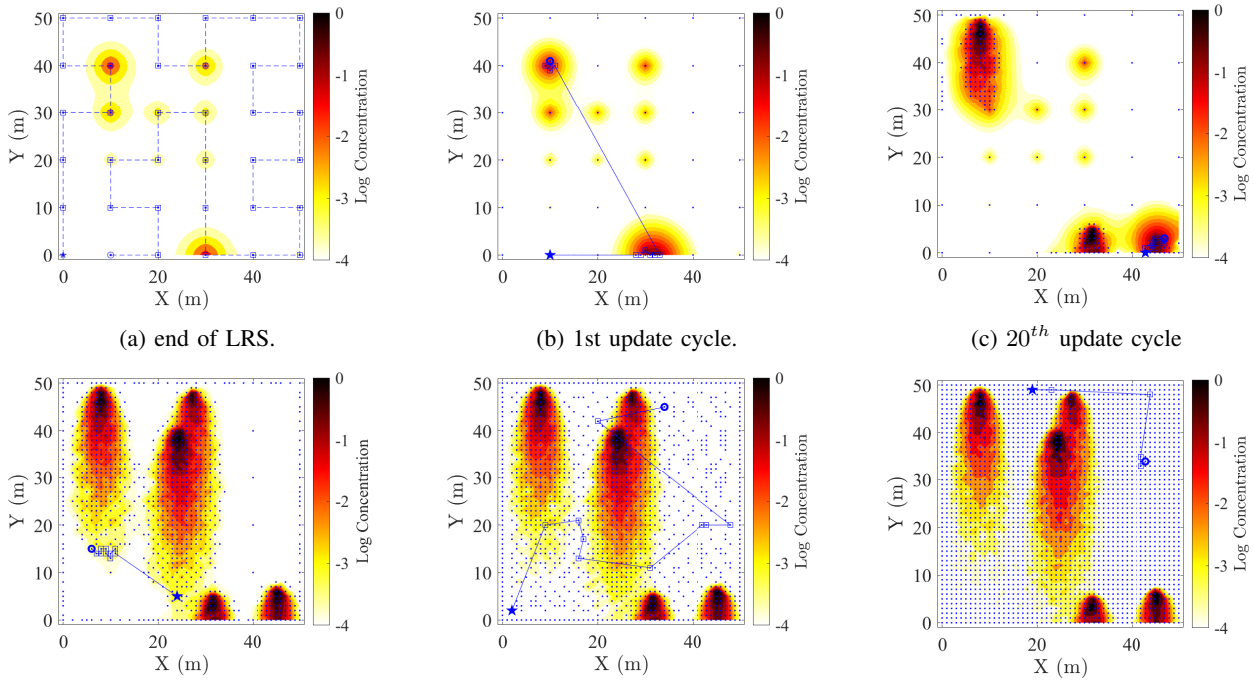

(a) end of LRS. (b) 1st update cycle. (c) 20^{th} update cycle

(d) 100^{th} update cycle (e) 150^{th} update cycle (f) End of HRS

Fig. 3: Estimated gas distribution map at different time instants, overlaid with the robot trajectories starting from the star marked cell and ending on a circle marked cell. Moreover, the sampled locations are highlighted by a blue dot marker, whereas, the sampling locations in the current phase(or update cycle) are highlighted by a square marker.

A. *Illustrative simulation*

To illustrate the scenario, the resulting ground truth gas distribution have been plotted in Fig 2. The ground truth data with added noise will be used as measurement samples obtained by the robot for the simulation study.

The region $\mathcal{D}$ is assumed to discretised in square cells of side length 1m. The choice of 1m is based on the assumption that the variation in concentration across a span of 1m is slower than the noise of the sensor. Furthermore, α is chosen to be 10 to generate the low resolution graph $\mathcal{G}_{LRS}$. Moreover, the algorithmic parameters M and T are chosen as 15 and 10 respectively, for the high resolution sampling phase. This means that the number of elements in Ω to be evaluated for each update cycle are 3003. The robot is assumed to move at a speed of 5 m/s and the sampling time t_{sam} is chosen to be 2 sec, based on the response of PID sensors, commonly used in mobile robotic gas sampling tasks [20]. The map update time t_{up} is chosen to be 50 sec.

The illustrative simulation results are presented in Fig. 3, when setting the reward r_i as the upper confidence bound (UCB) of the predicted gas concentration and associated variance, where $r_i = \mu_i + \beta\sigma_i^2$ with β is a scaling factor. The distance travelled and total time taken in the LRS phase are 350m and 142 sec respectively, resulting in the low resolution map as shown in Fig. 3a. Furthermore, the gas distribution maps after different map update cycles are presented in Figs. 3b - 3f. It can be noted from Fig. 3b that the two high concentration regions, based on the low resolution map of Fig. 3a, are sampled first, followed by further dense sampling of these regions in the upcoming update cycles. The UCB reward is inherently designed to perform exploitative spatially dense sampling upon encountering a high concentration region. Whereas, after sampling the high concentration plume region of a discovered source, the proposed algorithm chose the next sampling cells in a spatially diverse manner from the list of the unsampled cells due to the presence of the variance in r_i. Such a feature makes the proposed algorithm more suitable for mapping applications where little prior knowledge of the environment is available. The advantages of the proposed low-high resolution approach will be further clarified in the comparison study in the next subsection.

B. *Comparison study*

In this subsection, we compare the performance of the proposed algorithm with the baseline, a traditional sweep pattern, alongside different reward functions.

The first version randomly selects T cells from $\mathcal{Q}_u$ such that the inequality constraint of (P2) is not violated. In other words, the r_i is randomly assigned. However, due to the random nature of the cell choice, there could be a scenario where no feasible set of T cells may exists. In such a case, the robot randomly chooses a subset of T cells that satisfy the inequality. This is named constrained random sampling (CRS) and will show why using a focused reward based planner will give superior results. The second and third versions calculate the reward as the predicted concentration and UCB calculated from the GMRF, respectively. This will

show the performance of the proposed algorithm for a greedy (concentration based) or balanced (UCB) reward based path planner. The fourth and fifth versions also calculate the reward as the predicted concentration and UCB from the GMRF, respectively. However, they do not consider any LRS information. In other words, no LRS is performed and the HRS phase is started with just a single measurement sample at the starting location. This will demonstrate the advantages of performing the LRS to generate a prior for the HRS phase.

To remove any bias towards a given scenario, 20 Monte Carlo (MC) simulations are run for each of the algorithms, consisting of 4 different starting configurations each with 5 sets of randomised source scenarios. The starting locations are chosen as the 4 corners of the search domain. The source parameters are randomised around the values in Table I, and the same set of randomised sources are used for each algorithm. The metrics used for comparing the performance of the proposed algorithm are: the overall distance travelled by the robot, the root mean squared error (RMSE) between the estimated gas distribution and the ground truth over time, and the time of RMSE convergence to its steady state value, all averaged over the 20 MC runs.

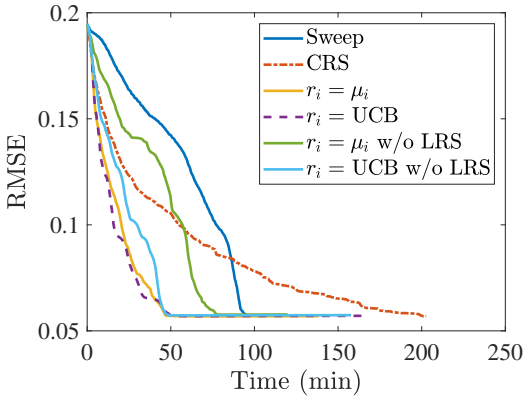

Fig. 4: Averaged RMSE of the inferred concentrations against the ground truth values over the 20 MC runs.

TABLE II: Total traveled distance and RMSE Convergence time (RMSE-CT) for different sampling protocols

	Distance (m)	(RMSE-CT) (min)
Sweep	**2601**	95.33
CRS	34,807	202.72
$r_i = \mu_i$	15,547	**46.71**
r_i =UCB	24,065	51.41
$r_i = \mu_i$ w/o Prior	9,939	78.07
r_i = UCB w/o Prior	21,321	49.13

The RMSE over time for different sampling protocols are plotted in Fig. 4. It can be seen from Fig. 4 that the average RMSE between the predicted gas distribution and the ground truth over $\mathcal{D}$ converges quickly for the proposed LHR-GDM framework with $r_i = \mu_i$ and r_i = UCB as compared to the randomised sampling or sweep based sampling protocol. The quick reduction in the RMSE can be attributed to the inherent exploitative sampling feature upon encountering a high concentration region as discussed previously. Furthermore, such an exploitative dense sampling behaviour is more desirable in practical scenarios where resources (such as operation time) are limited, as the potentially unsampled high concentration regions based on the current belief are given priority at any given time.

The travel distance and the RMSE convergence time (includes the LRS phase where applicable) for different sampling procedures are tabulated in Table II. The sweep based sampling procedure required the least distance of all the compared sampling protocols. However, the RMSE convergence of the proposed LHR-GDM framework with either reward function results in a significant initial reduction of RMSE, along with convergence to a similar final RMSE approximately 45 mins before the sweep based sampling, and 150 mins before the CRS sampling procedure. Moreover, the proposed framework also requires significantly less travel distance as compared to random sampling during the mission, which demonstrates that a focused reward function under the proposed framework provides significant advantages to traditional sweep or random sampling protocols. It can also be seen from Fig. 4 that performing the LRS survey speeds up the convergence rate of the RMSE as compared to the simulation trials without a LRS. Therefore, it can be concluded that having a low resolution prior map based on the user knowledge for a coverage survey is beneficial, even allowing an exploitative reward, $r_i = \mu_i$, to have a similar convergence rate as UCB but with less travelling distance. The significant difference in the RMSE convergence times between $r_i = \mu_i$ and UCB without LRS emphasizes the explorative *edge* in performance provided by the LRS phase.

V. Conclusion and Future Work

This paper proposes an informative path planning algorithm that autonomously guides a robot to map the gas distribution in a region of interest. The LHR-GDM framework first generates a low resolution map to serve as a prior for the second phase, which performs dense sampling of the region. The dense sampling phase identifies the best T-cell path from an M cell candidate set, such that as many potentially high reward regions are sampled while ensuring that chosen T cells can be reached within the used specified time constraint. A simulation study demonstrated the *exploitation-exploration like* behaviour of the proposed algorithm, which on encountering a relatively high concentration region performs its exploitative dense sampling, followed by exploring outwards from previously sampled region until all the cells have been sampled once. A comparison study also demonstrates the advantages of performing the LRS in terms of quick resolution of key features of the map, along with the benefits of specific reward functions.

The LHR-GDM requires optimising over a combinatorial large set Ω for large values of M and T which can be computationally expensive. Exploring the probabilistic approaches in constructing the Ω set along with accounting for effects of wind could be an interesting direction of future research.

REFERENCES

[1] A. Francis, S. Li, C. Griffiths, and J. Sienz, "Gas source localization and mapping with mobile robots: A review," *Journal of Field Robotics*, vol. 39, no. 8, pp. 1341–1373, 2022. [Online]. Available: https://onlinelibrary.wiley.com/doi/abs/10.1002/rob.22109

[2] A. Lilienthal and T. Duckett, "Building gas concentration gridmaps with a mobile robot," *Robotics and Autonomous Systems*, vol. 48, pp. 3–16, 8 2004.

[3] A. J. Lilienthal, M. Reggente, M. Trincavelli, J. L. Blanco, and J. Gonzalez, "A statistical approach to gas distribution modelling with mobile robots - the kernel dm+v algorithm," in *2009 IEEE/RSJ International Conference on Intelligent Robots and Systems*, 2009, pp. 570–576.

[4] M. Reggente and A. J. Lilienthal, "Using local wind information for gas distribution mapping in outdoor environments with a mobile robot," in *SENSORS, 2009 IEEE*, 2009, pp. 1715–1720.

[5] S. Asadi, M. Reggente, C. Stachniss, C. Plagemann, and A. J. Lilienthal, "Statistical gas distribution modeling using kernel methods," *Intelligent Systems for Machine Olfaction*, pp. 153–179, 2011.

[6] C. Stachniss, C. Plagemann, and A. J. Lilienthal, "Learning gas distribution models using sparse gaussian process mixtures," *Autonomous Robots*, vol. 26, no. 2, pp. 187–202, 2009.

[7] M. Hutchinson, P. Ladosz, C. Liu, and W.-H. Chen, "Experimental assessment of plume mapping using point measurements from unmanned vehicles," in *2019 International Conference on Robotics and Automation (ICRA)*, 2019, pp. 7720–7726.

[8] J. G Monroy, J.-L. Blanco, and J. Gonzalez-Jimenez, "Time-variant gas distribution mapping with obstacle information," *Autonomous Robots*, vol. 40, no. 1, pp. 1–16, 2016.

[9] *Efficient Spatial Prediction Using Gaussian Markov Random Fields Under Uncertain Localization*, ser. Dynamic Systems and Control Conference, vol. Volume 3: Renewable Energy Systems; Robotics; Robust Control; Single Track Vehicle Dynamics and Control; Stochastic Models, Control and Algorithms in Robotics; Structure Dynamics and Smart Structures; Surgical Robotics; Tire and Suspension Systems Modeling; Vehicle Dynamics and Control; Vibration and Energy; Vibration Control, 10 2012.

[10] J. Burgués, V. Hernández, A. J. Lilienthal, and S. Marco, "Smelling nano aerial vehicle for gas source localization and mapping," *Sensors*, vol. 19, no. 3, 2019.

[11] P. P. Neumann, M. Bennetts, and I. M. Bartholmai, "Adaptive gas source localization strategies and gas distribution mapping using a gas-sensitive micro-drone," *Technology (BMWi)*, vol. 4, no. 5, p. 6, 2012.

[12] L. Bing, M. Qing-Hao, W. Jia-Ying, S. Biao, and W. Ying, "Three-dimensional gas distribution mapping with a micro-drone," in *2015 34th Chinese Control Conference (CCC)*, 2015, pp. 6011–6015.

[13] P. P. Neumann, S. Asadi, A. J. Lilienthal, M. Bartholmai, and J. H. Schiller, "Autonomous gas-sensitive microdrone: Wind vector estimation and gas distribution mapping," *IEEE Robotics & Automation Magazine*, vol. 19, no. 1, pp. 50–61, 2012.

[14] C. Ercolani, L. Tang, A. A. Humne, and A. Martinoli, "Clustering and informative path planning for 3d gas distribution mapping: Algorithms and performance evaluation," *IEEE Robotics and Automation Letters*, vol. 7, no. 2, pp. 5310–5317, 2022.

[15] A. Gongora, J. Monroy, F. Rahbar, C. Ercolani, J. Gonzalez-Jimenez, and A. Martinoli, "Information-driven gas distribution mapping for autonomous mobile robots," *Sensors*, vol. 23, no. 12, 2023. [Online]. Available: https://www.mdpi.com/1424-8220/23/12/5387

[16] C. Rhodes, C. Liu, and W.-H. Chen, "Informative path planning for gas distribution mapping in cluttered environments," in *2020 IEEE/RSJ International Conference on Intelligent Robots and Systems (IROS)*, 2020, pp. 6726–6732.

[17] ——, "Scalable probabilistic gas distribution mapping using gaussian belief propagation," in *2022 IEEE/RSJ International Conference on Intelligent Robots and Systems (IROS)*, 2022, pp. 9459–9466.

[18] ——, "Structurally aware 3D gas distribution mapping using belief propagation: A real-time algorithm for robotic deployment," *IEEE Transactions on Automation Science and Engineering*, pp. 1–15, 2023.

[19] G. Laporte and Y. Nobert, "A cutting planes algorithm for the m-salesmen problem," *Journal of the Operational Research society*, vol. 31, pp. 1017–1023, 1980.

[20] C. Rhodes, C. Liu, and W.-H. Chen, "Autonomous source term estimation in unknown environments: From a dual control concept to uav deployment," *IEEE Robotics and Automation Letters*, vol. 7, no. 2, pp. 2274–2281, 2022.